Journal of Materials Chemistry B

Accepted Manuscript

ROYAL SOCIETY OF CHEMISTRY

www.rsc.org/materialsB

Cite this: DOI: 10.1039/c0xx00000x

www.rsc.org/xxxxxx

ARTICLE TYPE

Core-shell structured Gd_2O_3:Ln@*m*SiO_2 hollow nanospheres: synthesis, photoluminescence and drug release properties

Rumin Li, Lei Li, Yunhua Han, Shili Gai,* Fei He, and Piaoping Yang*

Received (in XXX, XXX) Xth XXXXXXXXX 20XX, Accepted Xth XXXXXXXXX 20XX

DOI: 10.1039/b000000x

Gd_2O_3:Ln@*m*SiO_2 hollow nanospheres (Gd_2O_3:Ln hollow spheres coated by mesoporous silica layer) were successfully synthesized through a self-template method using $Gd(OH)CO_3$ as template to form a kind of hollow precursors (named HPs), which involved the incorporation of rare earth compound into the internal of the hydrophilic carbon shell , followed by the coating a mesoporous silica shell, and the subsequent calination in air. X-ray diffraction (XRD), scanning electron microscopy (SEM), transmission electron microscopy (TEM), Fourier transformed infrared (FT-IR), thermogravimetric and differential thermal analysis (TG-DTA), photoluminescence spectroscopy, kinetic decays as well as N_2 adsorption/desorption were employed to characterize the composites. The result indicates that the uniform Gd_2O_3:Ln@*m*SiO_2 composite with the particle size around 300 nm maintains the spherical morphology and good dispersibility of the precursor. Interestingly, the composite has double-shell structure including an inner shell of Gd_2O_3 and an outer shell of mesoporous silica. Moreover, they also exhibit respective bright red (Eu^{3+}, $^5D_0 \rightarrow {}^7F_2$) down-conversion (DC) emission and characteristic up-conversion (UC) emissions of Yb^{3+}/Er^{3+}. Under beams excitation, the hollow structured sample emerges emissions which should have potential application in biomedicine and other fields.

1. Introduction

Currently, synthesis of hollow spheres have become the hot spot of scientific research due to the outstanding properties of hollow structure, especially the ones shown in various areas like catalysis,[1] photonics,[2] fillers,[3] and biotechnology.[4] In general, the synthetic methods toward hollow spheres can be sorted into two types: template-free strategies and template strategies. The template-free strategies mainly relied on various well-known phenomena such as Ostwald ripening,[5] Kirkendall effect[6] and oriented attachment,[7] which all have been widely employed for fabricating the hollow spheres. Template strategies often employ sacrificial cores to obtain hollow spheres. For example, using PS spheres,[8,9] carbon spheres,[10] PMMA,[11] SiO_2[12] or resin[13] as sacrificed templates to obtain hollow TiO_2,[14] MnO_2,[15] Al_2O_3,[16] Cr_2O_3,[17] SnO_2[18] spheres. Need to mention, the removal of sacrificial cores in templates may cause environmental problem as a result of the product of calcination or the etching agents (acid or base). It is noteworthy that there are some kinds of new routes proposed to fabricate hollow micro- and nanospheres of hybrid materials, such as heterophase polymerization combined with the sol-gel process,[19] layer-by-layer method,[20] and gas bubble assisted approach.[21] Although much effort towards the preparation of hollow materials has been made, the synthesis of well-defined rare earth oxide hollow spheres has relatively less been studied and the procedure adopted at present, in some case, is complicated and the yields of hollow products are very low. In addition, the obtained product cannot be utilized for further application due to the lack of surface modification and functionalization. Hence, a facile, economic and green method to synthesize rare earth hollow materials for large-scale industrial preparation with defined shape multiple properties (luminescent, magnetic and electrical properties) should be highly promising.

As known to us, rare earth materials have been applied in high performance luminescent,[22] optoelectronic devices,[23] sensors,[24] MRI contrast agents devices[25] and bio-labling[26] owing to the large Stökes shifts, narrow emission bandwidths, long fluorescence lifetimes and suitability for multiphoton excitation.[27–29] Among all the rare earth oxides, cubic phase gadolinium oxide is an ideal luminescent host material because of its low phonon energy, favourable chemical durability, good thermal stability, and the ability of being easily doped with rare earth ions.[30–34]As an important member of rare earth material, Gd_2O_3 phosphors with various morphologies such as one-dimensional nanostructures like nanorods, nanotubes, nanowire, 3-dimensional flower, zero-dimensional nanoparticles have been valued and synthesized by a variety of techniques.[35–39] Besides, some nano- and micro- hollow spheres are much more seductive because of their low effective densities, large inner volume, transparent to visual light and so on.[40–42] However, the hollow products of Gd_2O_3 usually exert poor monodispersity and uniformity, and research on employing rare earth ions as dopants to develop their hollow structure with luminescent properties for many different uses is very uncommon. In order to extend the area of synthetic technique for hollow luminescent materials and overcome the shortness of traditional template methods, it is desirable to raise a simple, environmental and undemanding method for the synthesis of hollow, spherical and Ln-doped Gd_2O_3 phosphors, which are well-dispersed, uniform, multicoloured and spherical Gd_2O_3 nanosized phosphors. Meanwhile, the mesoporous silica which can endow different structures with a variety of attractive features, including good

biocompatibility, low toxicity, large pore volume, very high surface area has been applied in various synthetic process.[43–45]

Herein, we report a facile and green routine for the synthesis of Gd_2O_3:Ln@$m$$SiO_2$ hollow nanospheres through a self-template method to prepare hollow precursor and then mesoporous silica coating process was employed using CTAB as surfactant, followed by a calcination process to remove CTAB and carbon element. And the hollow precursors (named HPs) were formed through a self-template method using $Gd(OH)CO_3$ as template, which involved the precipitation of Gd^{3+} ions inside the inner carbon shell. Notably, silica shell can serve as outer mould to avoid the damage of inner Gd_2O_3:Ln shell during the calcination process and obviously enhance the chemical stability and photoluminescent stability of this material. The formation process and photoluminescent properties have been well characterized by various analysis techniques. It is worth noting that an influence on the colloidal stability of the primary particles formed is proceeded in hydrothermal condition without using any other controllable conditions. Because of simple, economical and environmentally friendly feature of this fabrication method, it may exert large potential and wide applications in the synthesis of other luminescent hollow spheres. We expect that this hollow inorganic luminescent sphere coated mesoporous silica can be well employed in various fields especially drug-delivery and target applications in the future.

2. Experimental section

2.1. Materials and synthesis

Analytical grade glucose, TEOS (95%), hexadecyl trimethyl ammonium bromide (CTAB), urea, and HNO_3 were purchased from Beijing chemical Corporation and used as received without further purification, Analytical grade Gd_2O_3, Eu_2O_3, Yb_2O_3, Er_2O_3 were purchased from Sinopharm Chemical Reagent Co., Ltd.

Preparation of $Gd(OH)CO_3:Eu^{3+}$. $Gd(OH)CO_3:Eu^{3+}$ were synthesized through urea-assisted homogeneous precipitation method. In a typical synthesis procedure, 0.95 mmol Gd_2O_3 and 0.05 mmol Eu_2O_3 were dissolved in 2 mol·L^{-1} of HNO_3 with stirring. The superfluous HNO_3 was driven off by heating treatment until the pH value of the solution reached between 2 and 3. The as-prepared $Gd(NO_3)_3$ and $Eu(NO_3)_3$ aqueous solution was added to 200 mL of deionized water. Subsequently, 12.01 g of urea was dissolved in the solution under vigorous stirring. The mixture was transferred into a flask and stirred at 85 °C water bath for 4 h. Finally, the product was washed by deionized water and ethanol several times and dried at 60 °C in air for 12 h.

Synthesis of HPs. In a typical process for the synthesis of HPs under hydrothermal condition, 1.6 g of glucose was dissolved in a mixture of 18 ml of deionized water and 12 mL ethanol. Then 200 mg of the obtained $Gd(OH)CO_3:Eu^{3+}$ were added, followed by vigorous stirring. The resulting suspension was transferred to a 50 ml Teflon autoclave and heated at 190 °C for 14 h. After that, the samples were washed with deionized water and ethanol several time and dried in air at 60 °C for 12 h.

Silica coating process. The coating process is completed via a modified stöber method. In a typical procedure, 0.2 g of HPs was ultrasonically dispersed in a mixed solution containing 50 mL of ethanol and 70 mL of deionized water. Subsequently, 0.3 g CTAB and 1.0 M concentrated ammonia aqueous solution were added to the mixed solution. After stirring at room temperature for 6 h, the product was washed with deionized water and ethanol several time and dried in air at 60 °C for 12 h. Finally, the sample was dried in the air and calcined in air at 800 °C for 3 h. Through this procedure, the $Gd_2O_3:Eu^{3+}$ hollow spheres coated with mesoporous silica were obtained. And the hollow Gd_2O_3:Ln@$m$$SiO_2$ (Ln = Yb^{3+}/Er^{3+}) were prepared by a similar process.

For comparison, $Gd_2O_3:Eu^{3+}$ and $Gd_2O_3:Yb^{3+}/Er^{3+}$ particles with the same doping composition were obtained by a similar urea-assisted precipitation followed by calcination process.

2.2. Drug loading and release study

The as-prepared hollow $Gd_2O_3Yb^{3+}/Er^{3+}$@$m$$SiO_2$ samples were employed as a drug carrier to research the drug loading and release properties according to the previous reports with some modifications.[46–50] Doxorubicin (DOX) was selected as the model drug. Typically, 30 mg of $Gd_2O_3:Yb^{3+}/Er^{3+}$@$m$$SiO_2$ composite was added to 5 mL of phosphate buffer solution (PBS, pH = 7.4) with a DOX concentration of 0.5 mg mL^{-1} at room temperature, and soaked for 24 h under stirring in dark conditions, which was sealed to prevent the evaporation of the solution. The DOX loaded sample (DOX-Gd_2O_3:Ln@$m$$SiO_2$) was separated by centrifugation. The *in vitro* release test of DOX was performed by immersing loaded sample in the release media of PBS under gentle stirring in dark conditions and the immersing temperature was kept at 37 °C. In a typical procedure for determining the release amount, the buffer solution was withdrawn at predetermined time intervals and immediately replaced with an equal volume of fresh PBS to keep the volume constant. The amount of DOX released at certain set times was determined by UV-vis spectroscopy at a wavelength of 490 nm.

2.3. Characterization

X-ray diffraction (XRD) was obtained in the 2θ range of 5–70 °C using a Rigaku-Dmax 2500 diffractometer with Cu Kα radiation (λ = 0.15405nm). SEM images were obtained from a field emission scanning electron. Composition of the as-prepared samples was equipped with an energy-dispersive X-ray spectrum (EDS, JEOL JXA-840). TEM was carried out from a FEI Tecnai G^2 S-Twin transmission electron microscope with a field emission gun operating at 200 kV elucidate the dimensions and the structural details of the particles. Fourier transform IR (FT-IR) spectra were measured on a PerkinElmer 580B IR spectrophotometer using KBr pellet technique. Inductively coupled plasma (ICP) measurement (Thermo iCAP 6000 ICPOES) was performed to determine the exact doping concentration of Eu^{3+}. N_2 adsorption/desorption isotherm was performed at 77 K using a Micromeritics ASAP 3020 instrument. The UC emission spectra were obtained using a 980 nm laser from an OPO (optical parametric oscillator, Continuum Surelite, USA) as the excitation source and detected by R955 (HAMAMATSU) from 400 to 900 nm. All of the measurements were performed at room temperature.

3. Results and discussion

3.1. Phase, structure and morphologies

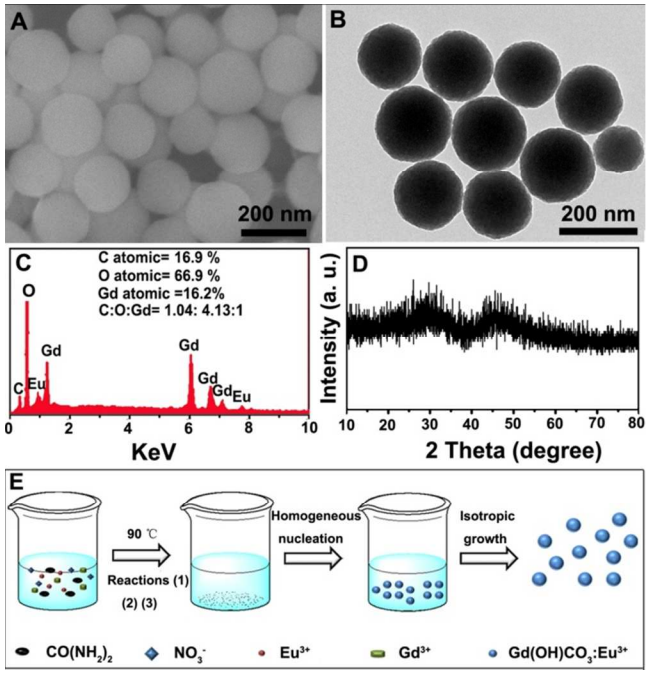

Fig. 1 FE-SEM image (A), TEM images (B), EDS (C), XRD (D) of as-prepared $Gd(OH)CO_3:Eu^{3+}$, and schematic illustration for the formation of $Gd(OH)CO_3:Eu^{3+}$ (E).

From the SEM image of the as-obtained $Gd(OH)CO_3:Eu^{3+}$ (Fig. 1A), we can see that the samples consist of uniform non-aggregated spherical particles with an average diameter of 220 nm and these particles present a smooth surface , which also can be clearly observed from the TEM image (Fig. 1B). The EDS spectrum (Fig. 2C) confirms the existence of carbon (C), oxygen (O), gadolinium (Gd), and europium (Eu) elements, and the atomic ratio of C: O: Gd was determined to be 1.04: 4.13: 1, which is in accordance with the stoichiometric atomic ratio of $Gd(OH)CO_3$. In addition, the content of Eu and Gd is determined by ICP-OES with the ratio about 5%, which is in accordance with the doping concentration mentioned above. As shown in the corresponding XRD pattern (Fig. 1D), there are just two broad peaks at about $2\theta = 32°$ and 48° and no other obvious diffraction peak, which can suggest the amorphous $Gd(OH)CO_3$ nature. In addition, the mechanism for the formation of $Gd(OH)CO_3$ particles have been concluded as shown in Fig. 1E.[51–53] The main reactions taking place in the water solution could be represented as follows:

$$CO(NH_2)_2 + H_2O \Leftrightarrow CO_2 + 2NH_3 \quad (1)$$

$$NH_3 + H_2O \Leftrightarrow NH_4^+ + OH^- \quad (2)$$

$$(0.95Gd^{3+},0.05Eu^{3+}) + 3OH^- + CO_2 \Rightarrow Gd_{0.95}Eu_{0.05}(OH)CO_3 + H_2O \quad (3)$$

As shown in Fig. 2A, the HPs have an average diameter of 250 nm, which have slightly increased size compared with $Gd(OH)CO_3:Eu^{3+}$ nanospheres. The enlarged particle size and hollow cavity can be assigned to the product formed by the reaction between glucose and $Gd(OH)CO_3:Eu^{3+}$ under hydrothermal condition at elevated temperature, which change the samples' internal microstructure and maintain the size of the product. As a result, the precursors' morphology converts from

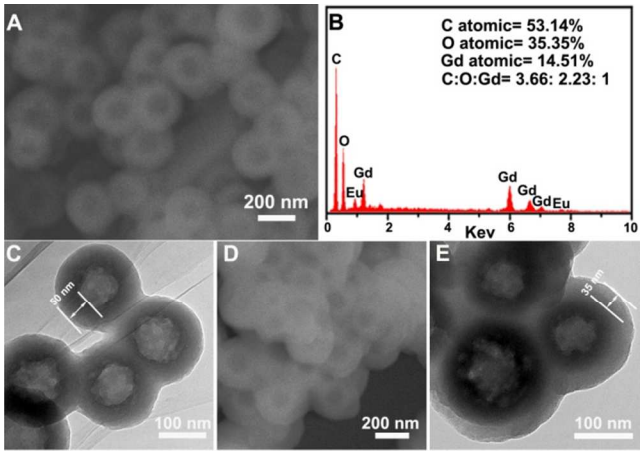

Fig. 2 FE-SEM images of HPs (inset is corresponding (B), TEM image (C); FE-SEM images (D) and TEM (E) image of precursor coating with silica; and EDS patterns (B) of as-synthesized HPs.

solid shape to hollow shape but the size of them does not change much. From the EDS of the as-prepared HPs (Fig. 2B), we can affirm the presence of the carbon (C), oxygen (O), gadolinium (Gd), and europium (Eu) elements. There is high signal of the carbon in the EDS pattern because ionic adsorption reaction of glucose with $Gd(OH)CO_3$ to form the compound ($Gd(Eu)(C_xH_yO_z)$) according to report,[54] which will be discussed in detail in the formation mechanism. The TEM image of HPs prepared from glucose exhibit a uniform size distribution and an apparent hollow structure, comprised of a shell which thickness is about 50 nm. Fig. 2D and E show that the HPs coating with silica still keep the morphological properties of them except for a larger particle size about 35 nm. Interestingly, the nanospheres exhibit more agglomerate appearance than the HPs, which may be caused by the coating of silica through the stöber sol–gel approach.

The morphology, nanostructure and the elemental composition of the hollow $Gd_2O_3@mSiO_2$ nanospheres are displayed in Fig 3. From the SEM images (Fig. 3A), the particles are composed of uniform spheres which are similar to HPs except for an increase size of diameter of inner cavity. The expansion of cavity volume should be attributed to the dehydration and oxygenolysis of the cross-linked structure of the shells and the densification of the precursor on the inner wall when converted to the closely compact oxides phosphors under calcination. The thickness of the shell is about 50 nm (inset in Fig. 3A), further confirming the shrinkage of the inner shell after annealing. Additionally, the obtained samples are of good dispersibility compared to the precursors. From the TEM image (Fig. 3D), we can see that the samples have an obvious double-shell structure and the intense contrast between the black margins and the bright centers of the spheres confirms the existence of hollow structures, which is consistent with the SEM result. The magnified TEM image (Fig. 3E) exhibits the detailed morphology of the sample. The thickness of the inner shells for the hollow spheres is estimated to be about 10 nm, better illustrating the conversion from the HPs to the Gd_2O_3 crystal. The EDS (Fig. 3B) of hollow $Gd_2O_3:Eu^{3+}@mSiO_2$ shows very weak carbon signal, which should be assigned to the carbon's burning off after annealing. The reduction of carbon is well consistent with TEM result: the dark area much thinner after calcining due to removal of carbon

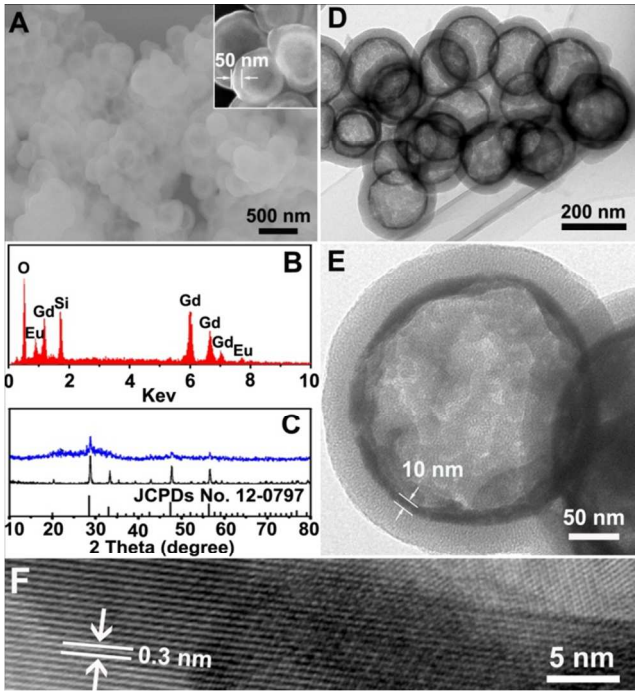

Fig. 3 FE-SEM images (A), EDS of Gd_2O_3:Eu^{3+}@*m*SiO_2 (B), XRD patterns of Gd_2O_3:Eu^{3+} solid spheres (black line) and Gd_2O_3:Eu^{3+}@*m*SiO_2 hollow nanospheres (blue line) (C), TEM image (D), magnified TEM image (E), and HRTEM image (F) of Gd_2O_3:Eu^{3+}@*m*SiO_2 composite.

element. According to the result of EDS, the black ring-like part (dark area) is assigned to Gd_2O_3:Eu^{3+} crystal. Fig. 3C shows the wide-angle XRD patterns of as-synthesized Gd_2O_3:Eu^{3+}@*m*SiO_2 composites and pure Gd_2O_3:Eu^{3+} spheres. All the diffraction peaks are in good agreement with the standard positions from the hexagonal Gd_2O_3 phase (JCPDs NO. 12-0797), and no diffractions from carbon and other phases coupled with the doped component can be detected, implying that high purity of the two samples. It can be seen that the intensity of the XRD patterns in hollow Gd_2O_3@*m*SiO_2 is much weaker in comparison to the pure Gd_2O_3:Eu^{3+} spheres, and the weak, broad band at 2θ=22° canbe assigned to the coating with the mesoporous silica shell. The pattern of as-prepared composites exhibits a relatively high intensity peak and two low reflections which can suggest that the cubic phase is still the diffraction width broadens apparently in the composites, indicating that the crystallinity of the Gd_2O_3 inner shell is smaller than the pure Gd_2O_3:Eu^{3+} NSs. Hence, the calcination process has a trebling function: the formation of hollow Gd_2O_3:Ln structures from the HPs, the removal of carbon element and the elimination of CTAB. The obvious lattice fringes in the HRTEM image (Fig. 3F) confirm the high crystallinity of the inner layer, which is in agreement with the XRD results. The distances of 0.30 nm between the adjacent lattice fringes agree well with the hexagonal Gd_2O_3 phase (JCPDS No.12–0797).

The functional groups on the as-synthesized Gd(OH)CO_3:Eu^{3+} precursor， HPs, Gd_2O_3:Eu^{3+}@*m*SiO_2 hollow nanospheres were examined by the FT-IR spectra, as shown in Fig. 4. In the FT-IR spectrum for Gd(OH)CO_3:Eu^{3+} (Fig. 4A), the broad absorption band at 3407 cm^{-1} can be attributed to the coupled effects of molecular water and free hydroxyl groups, and the four adsorption

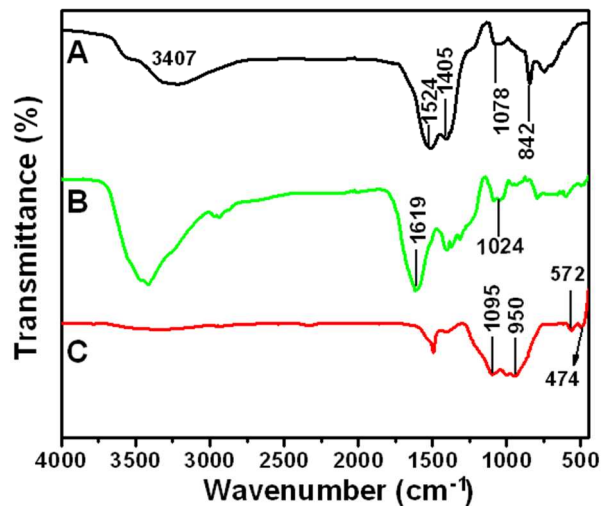

Fig. 4 FT-IR of as-prepared Gd(OH)CO_3:Eu^{3+} precursor (A), HPs (B), Gd_2O_3:Eu^{3+}@*m*SiO_2 hollow nanospheres (C).

bands 1524, 1405, 1078 and 842 cm^{-1} can be assigned to respective CO (ν_{as}), CO (ν_{as}), CO (ν_s) and CO (δ) in CO^{3-}groups, suggesting the composition of Gd(OH)CO_3:Eu^{3+}. It's worth noting in the FT-IR spectrum of HPs (Fig. 4B) that the OH^- and CO (ν_{as}) groups are reserved, and two new bands can be observed which is C=C (1619 cm^{-1}) and –C–O–C– linkage (1024 cm^{-1}). The presence of these two bands supports the polymerization reaction of glucose and the unsaturated C=C groups, indicating that a carbonization process has occurredduring the generation of HPs. The FT-IR spectrum of hollow Gd_2O_3:Eu^{3+}@*m*SiO_2 (Fig. 4C) shows that almost all of the functional groups related with the precursor disappear except forthe peaks assigned to Si-O-Si (1095 cm^{-1}), Si-OH (950 cm^{-1}) and Si-O (474 cm^{-1}), revealing that the complete transformation from the HPs to the hollow structure product and the successful coating of silica. Furthermore, a new band at 572 cm^{-1} can be assigned to the Gd(Eu)-O stretching adsorption, which also confirms the formation of Gd_2O_3:Eu^{3+} hollow spheres *via* the urea-based precipitation method and the further annealing process.

The conversion process from as-prepared pure Gd(OH)CO_3:Eu^{3+} precursor to the HPs, and then to the final Gd_2O_3:Eu^{3+}@*m*SiO_2 hollow structured nanospheres were explored *via* TG-DTA shown in Fig. 5, respectively. The insets are their corresponding DTA. It is shown that the TG curve of Gd(OH)CO_3:Eu^{3+} precursor (Fig. 5A) can be divided into two stages. And the TG curve of HPs@SiO_2 sample demonstrates that three steps of weight loss occur, as shown in Fig. 5B. The first slow weight loss before 200 °C should be associated with the physically adsorbed water on the surface of the product and the further dehydration and densification of inner complex layer. The sharp weight loss should be due to the burning of carbon and the decomposition of inner complex layer inside the inner surface of silica. And the removal of CTAB should result in the weight loss between 500 °C and 800 °C. It is worth noting that the weight loss of pure Gd(OH)CO_3:Eu^{3+} precursor is 27.1%, which is regarded as the as-formed Gd_2O_3:Eu^{3+} phosphors. While for the HPs@SiO_2, the residual weight percentage is 42.2%, which is regarded as hollow Gd_2O_3:Eu^{3+}@*m*SiO_2 sample. The results also reveal the

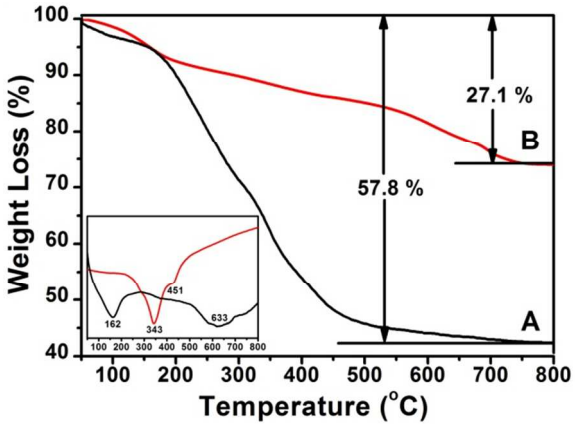

Fig. 5 TG curves of $Gd(OH)CO_3:Eu^{3+}$ precursor (A) and HPs coating with silica (B). Insets are their corresponding DTA curves.

high yield of the hollow products obtained by this method. The DTA of $Gd(OH)CO_3:Eu^{3+}$ (inset in Fig. 5) shows two peaks during the calcination process. The first one can be attributed to the physically adsorbed water on the surface of the precursor. The second peak can be ascribed to the decomposition of the $Gd(OH)CO_3:Eu^{3+}$ precursor to form $Gd_2O_3:Eu^{3+}$ nanocrystals. As shown in Fig. 5B for DTA of the HPs@SiO_2, there is just one obviously sharp peak in the curve compared with two peaks of $Gd(OH)CO_3:Eu^{3+}$ precursor. It may be explained that the degradation of the composite nanospheres need high temperature, which can also confirm the formation of the complex and the loss of the $Gd(OH)CO_3:Eu^{3+}$ after hydrothermal reaction. In addition, the removal of CTAB is manifested by the temperature of 451 °C. The burning of this material releases lots of energy during the calcining process and afford the formation of Gd_2O_3:Ln.

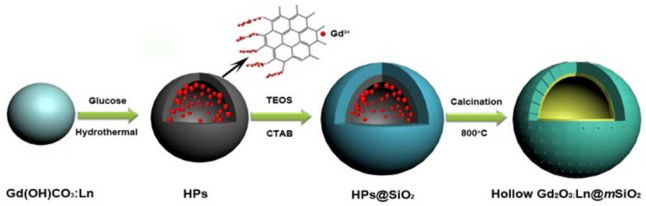

Scheme 1 Schematic illustration for the possible formation mechanism of HPs, and final Gd_2O_3@$m$$SiO_2$ hollow spheres.

3.2. Formation and growth mechanism

We employed Scheme 1 to depict a possible mechanism for the formation of $Gd_2O_3:Eu^{3+}$@$m$$SiO_2$ hollow nanospheres according to the above XRD, SEM, TEM, TG/DTA, and FT-IR analysis. Above all, it is the fabrication of $Gd(OH)CO_3$:Ln and the possible mechanism has been mentioned above. The HPs were obtained using a self-template method and the formative mechanism is proposed as follows: Firstly, the carbonization of the glucose. In this step, glucose converts to colloid carbon shell and encapsulate the $Gd(Ln)(OH)CO_3$ template in the hydrothermal process. With the proceeding of the hydrothermal reaction, the electronegative bonds hydroxy and carbonyl emerge inside the colloid shell from the carbonization, initiating coordination reaction with Gd^{3+} (Ln) ions on the surface of $Gd(OH)CO_3$ spheres to form complexes Gd(Ln)(CxHyOz). Meanwhile, $Gd(OH)CO_3$ dissolves to Gd^{3+}, OH^-, and CO_3^{2-} (precipitation and dissolution equilibrium: $Gd(Ln)(OH)CO_3 \Leftrightarrow Gd^{3+}(Ln) + OH^- + CO_3^{2-}$). Due to Gd^{3+} ions precipitate inside the inner carbon shell by coordination bond and hydrogen bond, the dissolution of the $Gd(Ln)(OH)CO_3$ and the growth of the hollow spheres Gd(Ln)(CxHyOz) occurred simultaneously throughout the continuous reaction. Subsequently, the HPs are coated by a further layer of mesoporous silica through a simple process using CTAB as template. Composite nanospheres HPs@SiO_2 converts to hollow Gd_2O_3:Ln@$m$$SiO_2$ by the heating treatment. The conversion can divided into two sections during the calcination process. On one hand, carbon skeleton dehydrates and oxidized into CO_2. On other hand, Gd^{3+} ions absorbed inside the carbon shell extend towards the silica with removal of carbon skeleton and oxidized into $Gd_2(Ln)O_3$. ($Gd(Ln)(CxHyOz) + O_2 \Leftrightarrow Gd_2(Ln)O_3 + CO_2 + H_2O$). Furthermore, the elimination of CTAB has taken place at the same time. Finally, hollow Gd_2O_3:Ln@$m$$SiO_2$ nanospheres are obtained.

3.3. Luminescence properties.

Fig. 6A gives the PL excitation (left) and emission (right) spectra of $Gd_2O_3:Eu^{3+}$@$m$$SiO_2$. The excitation spectrum (Fig. 6A, left) tested by the Eu^{3+} $^5D_0 \rightarrow {}^7F_2$ transition at 613 nm for $Gd_2O_3:Eu^{3+}$@$m$$SiO_2$ shows that a strong, broad band appears at about 257 nm which is attributed to the excitation of the oxygen-to-europium charge transfer band (CTB), and some weak lines in the longer-wavelength region can be due to the f–f transitions of the Gd^{3+} and Eu^{3+}. Upon excitation of 257 nm, The emission spectrum of $Gd_2O_3:Eu^{3+}$@$m$$SiO_2$ exhibits four main groups of emission lines at 538, 593, 613 and 651 nm, which are assigned to $^5D_1 \rightarrow {}^7F_1$ and $^5D_0 \rightarrow {}^7F_j$ (j = 1, 2, 3) transitions of Eu^{3+}, respectively. Apparently, the emission spectrum is dominated bythe red $^5D_0 \rightarrow {}^7F_2$ transition of the Eu^{3+}, which is an electric-dipole allowed transition and hypersensitive to the environment.[52] The luminescence decay curves of $Gd_2O_3:Eu^{3+}$@$m$$SiO_2$ hollow micorsphres are presented in Fig. 6B, it can be seen that the decay curve can be well fitted into single-exponential function as $I(t) = I_0\exp(-t/\tau)$ (I_0 is the initial emission intensity at t = 0, and τ is the 1/e lifetime of the emission center). The average lifetime of the Eu^{3+} ions can be determined to be 2.85 ms, which becomes longer in comparison to that of $Gd_2O_3:Eu^{3+}$ according to the literatures of our group.[52] The reason is that some of Eu^{3+} ions on the surface of Gd_2O_3 could diffuse into amorphous silica, which could lead to the increase of non-radiative transition rate of Eu^{3+}, and there are a large number of OH bonds and disorder the lattices in the silica shell.[45] Fig. 6C shows the PL emission spectra of $Gd_2O_3:Eu^{3+}$ spheres and $Gd_2O_3:Eu^{3+}$@$m$$SiO_2$ hollow nanospheres under the same excitation. The emission spectrum of $Gd_2O_3:Eu^{3+}$@$m$$SiO_2$ is very similar to that of $Gd_2O_3:Eu^{3+}$, except for a decrease of the intensity. It is notable that the extra $^5D_0 \rightarrow {}^7F_2$ emission lines at 622 nm emerges strongly, implying the emissions of Eu^{3+} ions adhere to amorphous phased materials in the emission spectrum of $Gd_2O_3:Eu^{3+}$@$m$$SiO_2$. It may indicate that some of Eu^{3+} locating in the lattices of $Gd(OH)CO_3$ disperse into the silica shells and on the surface of Gd_2O_3 nanoparticles under the condition of calcination, and the dispersal of Eu^{3+} locates on the red side of the charge bands.

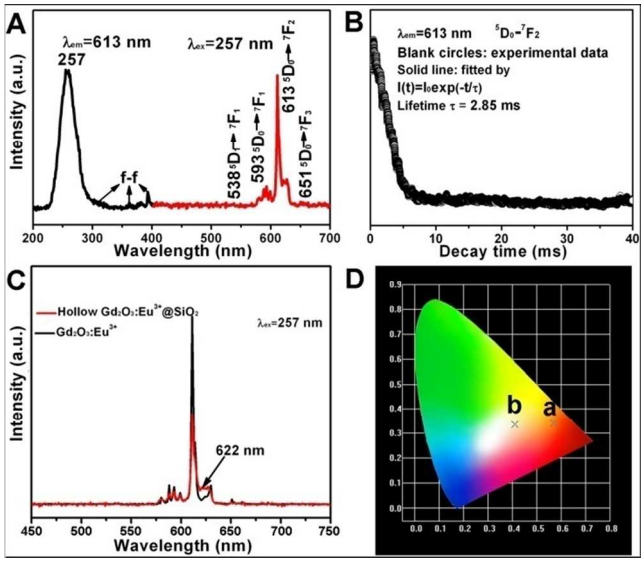

Fig. 6 Excitation (left) and emission spectra (right) of Gd_2O_3:Eu^{3+}@$m$$SiO_2$ hollow nanospheres (A); luminescence decay curves of Gd_2O_3:Eu^{3+}@$m$$SiO_2$ hollow nanospheres (B); emission spectra (C) and CIE chromaticity (D) of Gd_2O_3:Eu^{3+} and Gd_2O_3:Eu^{3+}@$m$$SiO_2$ hollow nanospheres.

The up-conversion (UC) luminescence spectra of hollow Gd_2O_3:Yb^{3+}/Er^{3+}@$m$$SiO_2$ recorded in 400-750 nm region under 980 nm laser excitation is shown in Fig. 7.Fig. 7A shows the UC emission spectrum of the Gd_2O_3:Yb^{3+}/Er^{3+}@$m$$SiO_2$ sample. The emission bands centered at 522, 538 and 661 nm can be ascribed to $^2H_{11/2}$→$^4I_{15/2}$ (green), $^4S_{3/2}$→$^4I_{15/2}$ (green) and $^4F_{9/2}$→$^4I_{15/2}$ (red) transitions of Er^{3+}, respectively.[55-57]It is obvious that the emission intensity of the composites shows quite large Stark splitting on account of large crystal field of Gd_2O_3 matrix in composites. This phenomenon can certify that the rare earth oxide is of great crystallization after calcination procedure. The emission spectra of Gd_2O_3:Yb^{3+}/Er^{3+} spheres and Gd_2O_3:Yb^{3+}/Er^{3+}@$m$$SiO_2$ hollow nanospheres are shown in Fig. 9B. As shown, the shape of emission spectrum of the hollow sample is almost same to that of Gd_2O_3:Yb^{3+}/Er^{3+}, while the intensity has an obvious reduction, which should be ascribed to the coating of mesoporous silica. It is noteworthy that comparing with the Gd_2O_3:Eu^{3+} spheres, the hollow material still shows high up-conversion luminescent stability and high excitation efficiency. Furthermore, the up-conversion mechanism of Gd_2O_3:Yb^{3+}/Er^{3+}@$m$$SiO_2$ is presented in Fig. 7D. Under 980 nm excitation, the Yb^{3+} absorbs the photon and promotes to its excited $^2F_{5/2}$ state.[55] The energy of Yb^{3+} ion $^2F_{5/2}$ state can transfer to a ground state ($^4I_{15/2}$) electron of Er^{3+}, and some of the excited ions decay to the low-lying level of $Er^{3+4}I_{13/2}$. On the one hand, a second photon transferred by the excited Yb^{3+} promotes a non-radiative decay to the low-lying $^4F_{7/2}$, $^4F_{9/2}$, and $^5F_5$ of the Er^{3+}.[58-61]

The respective CIE coordinates for the emission spectra of Gd_2O_3:Eu^{3+} and Gd_2O_3:Yb^{3+}/Er^{3+} with pure samples and hollow structured samples are shown in Fig. 6D and Fig. 7C. As shown in the different diagram, the different CIE chromaticity values are ascribed to weaken intensity ratios for the products, which should be caused by the hollow interior and mesoporous silica outside.[62–64]

3.4. Bifunctional drug carrier and the release property

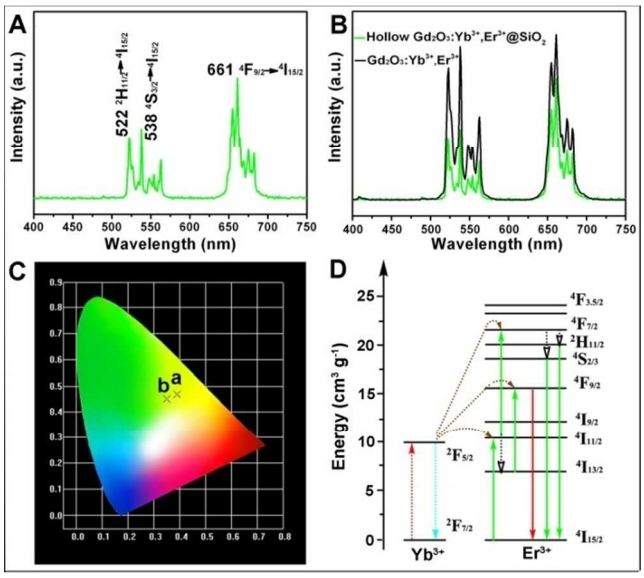

Fig. 7 NIR-to-visible UC emission spectra of Gd_2O_3:Yb^{3+}/Er^{3+}@$m$$SiO_2$ (A); emission spectra of Gd_2O_3:Yb^{3+}/Er^{3+} spheres and Gd_2O_3:Yb^{3+}/Er^{3+}@$m$$SiO_2$ (B); CIE chromaticity of Gd_2O_3:Yb^{3+}/Er^{3+} spheres and Gd_2O_3:Yb^{3+}/Er^{3+}@$m$$SiO_2$ hollow spheres; and proposed energy transfer mechanisms under 980 nm diode laser excitation in Gd_2O_3:Yb^{3+}/Er^{3+}@$m$$SiO_2$ hollow spheres (D).

The bifunctional (mesoporous, luminescent) drug carrier, Gd_2O_3:Yb^{3+}/Er^{3+}@$m$$SiO_2$, was prepared using inner Gd_2O_3:Yb^{3+}/Er^{3+} as the luminescent component, and the mesoporous property was obtained by a CTAB-template procedure. N_2 adsorption/desorption isotherm of samples is depicted in the Fig. 8. It can be seen that the sample shows typical IV isotherm with H_1-hysteresis loops, revealing the mesoporous structure of the sample. The relatively wide pore size distributions (inset of Fig. 8) should be ascribed to the unique structures with large interior space and small pores in the mesoporous shell. The respective BET surface area, average pore size, and the pore volume of samples is calculated to be 154.8 $m^2 \cdot g^{-1}$, 11.173 nm, and 0.522 $cm^{-3} \cdot g^{-1}$, which are suitable for loading drug molecules.

We used DOX as a model drug to investigate the drug storage and release properties of Gd_2O_3:Yb^{3+}/Er^{3+}@$m$$SiO_2$ hollow spheres. According to previous reports,[65–68] the DOX molecules are entrapped within the mesopores by an impregnation process and liberated *via* a diffusion-controlled manner. Hence, the Si–OH groups on the mesoporous layer surface can form hydrogen bonds with the carboxyl groups in the drug molecules. In the process of drug release, when the buffer solution permeated into the mesopores, the drug was dissolved into PBS and bursts from the composite through the mesoporous channels. The cumulative drug release profile of the DOX-Gd_2O_3:Ln@$m$$SiO_2$ system as a function of release time in the release media of PBS with different pH values is shown in Fig. 9. It can be observed that the release profile exhibits typical sustained properties. During the drug loading process, the DOX molecules may first be adsorbed onto the surface of the material in the impregnation procedure through hydrogen bonds. At pH=7, we can see obviously from the profile that the release of DOX was divided into two distinct

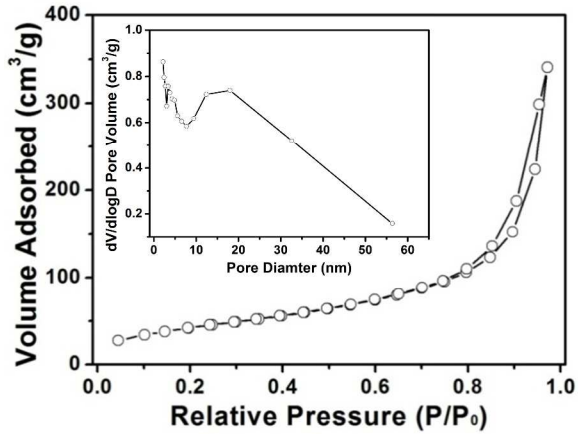

Fig. 8 N_2 adsorption/desorption isotherm of Gd_2O_3:Yb^{3+}/Er^{3+}@$m$$SiO_2$ hollow nanospheres. Inset is the corresponding pore size distribution.

stages: a burst release whose released amount reaches about 52% after 10 h and then a relatively slow trend. The sharp initial fast release can be attributed to the rapid leaching of the physically adsorbed drug molecules, which interact more weakly with the outer surfaces or near the pore entrances of the channels. And the slow release the rest of the DOX may be ascribed to the strong of interaction between DOX molecules and the inner surface. After 10 hours, the drug attached to the channels and inner surfaces will dissolve after the longer-time penetration of the medium and diffuse along aqueous pathways into the buffer solution. According to the analysis above, it can be deduced that the hollow Gd_2O_3:Ln@$m$$SiO_2$ system exhibits potential properties as a drug carrier for targeting systems in the drug delivery and disease therapy fields. For example, in the area of tumor treatment, the initial first burst of DOX release can significantly inhibit the tumour cell growth and achieve a sufficient initial dosage of the antitumour drug. Moreover, the sustained DOX release can be preferable to prevent the further proliferation of the cancer cells which survive the initial stage of the drug release.

Furthermore, the cumulative drug release from DOX-Gd_2O_3:Ln@$m$$SiO_2$ at lower value (pH = 4) was also be detected. As shown in Fig. 9, the drug releasing profile displays a similar trend as that of pH = 7, which should be due to the well accepted diffusion-controlled process. During the beginning of 1 h, 60.4% of DOX is released. Also, 76.3% of DOX has released after 40 h. Therefore, the drug release rate of DOX-Gd_2O_3:Ln@$m$$SiO_2$ composites is obviously pH-dependent and increases with the decrease of pH value. This trend can be attributed to the decreased pH weakens the bond energy and the electrostatic adsorption force with positively charged DOX molecules, resulting in the faster drug release rate. Considering the different pH values in blood plasma (pH = 7.4), in extracellular tumour matrix (pH = 5.8–7.2), and in the stomach (pH = 1.5–3.5), this carrier composites with pH-sensitive drug release property is promising to be a carrier for releasing anticancer drug after endocytosis by cancer cells.

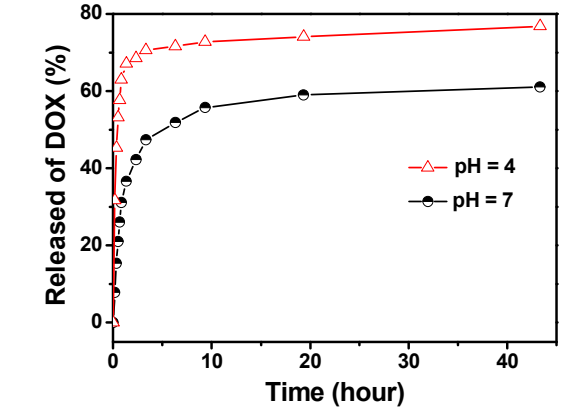

Fig. 9 Cumulative DOX release from the carrier at pH = 7 (black line), pH = 4 (red line).

4. Conclusions

In summary, Gd_2O_3:Ln@$m$$SiO_2$ (Ln = Eu^{3+} and Yb^{3+}/Er^{3+}) hollow nanospheres with a uniform diameter of 300 nm were successfully synthesized through a self-template method using $Gd(OH)CO_3$ as template and silica coating method which followed by a subsequent calcination process. An ionic adsorption of the hydrothermal carbonization of carbohydrates or an influence on the colloidal stability of the primary particles formed is proceeded in hydrothermal condition without any other controllable measure. And the whole fabrication process is completely green and suitable for inexpensive mass production of Gd_2O_3 hollow structure. The as-prepared Gd_2O_3:Ln (Eu^{3+} and Yb^{3+}/Er^{3+})@$m$$SiO_2$ exhibits strong and multicoloured DC and UC emissions under ultraviolet and NIR light excitation. In particular, due to their uniform hollow structure and mesoporous pores, the as-prepared Gd_2O_3:Ln@$m$$SiO_2$ (Ln = Eu^{3+} and Yb^{3+}/Er^{3+}) hollow nanospheres should have wide applications in biomedical field.

Acknowledgments

Financial supports from the National Natural Science Foundation of China (NSFC 21271053), Research Fund for the Doctoral Program of Higher Education of China (20112304110021), Natural Science Foundation of Heilongjiang Province (LC2012C10), Program for New Century Excellent Talents in University, Harbin Sci.-Tech. Innovation Foundation (RC2012XK017012), and the Fundamental Research Funds for the Central Universities of China are greatly acknowledged.

Notes and references

Key Laboratory of Superlight Materials and Surface Technology, Ministry of Education, College of Material Science and Chemical Engineering, Harbin Engineering University, Harbin, China. E-mail: yangpiaoping@hrbeu.edu.cn; gaishili@hrbeu.edu.cn.

1 J. G. Yu, G. P. Dai and B. B. Huang, *J. Phys. Chem. C*, 2009, **113**, 16394.
2 C. L. Yan and D. F. Xue, *J. Alloys Compd.*, 2007, **431**, 241.
3 M. Olek, J. Ostrander, S. Jurga, H. Mohwald, N. Kotov, K. Kempa and M. Giersig, *Nano Lett.*, 2004, **4**, 1889.
4 P. P. Yang, S. L. Gai and J. Lin, *Chem. Soc. Rev.* 2012, **41**, 3679.
5 H. G. Yang and H. C. Zeng, *J. Phys. Chem. B*, 2004, **108**, 3492.
6 Y. D. Yin, R. M. Rioux, C. K. Erdonmez, S. Hughes, G. A. Somorjai and A. P. Alivisatos, *Science*, 2004, **304**, 711.
7 A. W. Xu, Y. R. Ma and H. Colfen, *J. Mater. Chem.*, 2007, **17**, 415.
8 X. F. Song and L. Gao, *J. Phys. Chem. C*, 2007, **111**, 8180.

9 X. F. Wu, Y. J. Tian, Y. B. Cui, L. Q. Wei, Q. Wang and Y. F. Chen, *J. Phys. Chem. C*, 2007, **111**, 9704.
10 M. M. Titirici, M. Antonietti and A. Thomas, *Chem. Mater*., 2006, **18**, 3808.
11 Z. Y. Wang and A. Stein, *Chem. Mater.*, 2008, **20**, 1029.
12 D. K. Yi, S. S. Lee, G. C. Papaefthymiou and J. Y. Ying, Chem. Mater, 2006, **18**, 614.
13 H. G. Zhu and M. J. McShane, *Langmuir*, 2005, **21**, 424.
14 H. Strohm and P. Lobmann, *J. Mater. Chem.*, 2004, **14**, 2667.
15 J. Fei, Y. Cui, X. Yan, W. Qi, Y. Yang, K. Wang, Q. He and J. Li, *Adv. Mater.*, 2008, **20**, 452.
16 Y. Q. Jiang, X. F. Ding, J. Z. Zhao, B. Hari, X. Zhao, Y. M. Tian, K. F. Yu, Y. Sheng, Y. P. Guo and Z. C. Wang, *Mater. Lett.*, 2005, **59**, 2893.
17 A. B. Fuertes, M. Sevilla, T. Valdes-Solis and P. Tartaj, Chem. Mater., 2007, **19**, 5418.
18 W. M. Zhang, J. S. Hu, Y. G. Guo, S. F. Zheng, L. S. Zhong, W. G. Song and L. J. Wan, *Adv. Mater.*, 2008, **20**, 1160.
19 M. Yang, J. Ma, C. L. Zhang, Z. Z. Yang and Y. F. Lu, *Angew. Chem. Int. Ed*., 2005, **44**, 6727.
20 Y. Wang, A. S. Angelatos and F. Caruso, *Chem. Mater*., 2008, **20**, 848.
21 C. Yan and D. Xue, *J. Alloys Compd.*, 2007, **431**, 241.
22 C. X. Li, Z. W. Quan, J. Yang, P. P. Yang and J. Lin, *Inorg. Chem.*, 2007, **46**, 6329.
23 B. Yan and X. F. Qiao, *J. Phys. Chem. B*, 2007, **111**, 12362.
24 J. H. Hao, Y. Zhang and X. Wei, *Angew. Chem. Int. Ed*., 2011, **50**, 6876.
25 Y. Liu, D. Tu, H. Zhu, R. Li, W. Luo and X. Y. Chen, *Adv. Mater*., 2010, **22**, 3266.
26 Y. Wang, X. Bai, T. Liu, B. Dong, L. Xu, Q. Liu and H. Song, *J. Solid State Chem.*, 2010, **183**, 2779.
27 F. Auzel, *Chem. Rev*., 2004, **104**, 139.
28 K. Binnemans, *Chem. Rev*., 2009, **109**, 4283.
29 M. L. Sogin, H. G. Morrison, J. A. Huber, D. Mark Welch, S. M. Huse, P. R. Neal, J. M. Arrieta and G. J. Herndl, *Proc. Natl. Acad. Sci.*, 2006, **103**, 12115.
30 G. Jia, H. P. You, M. Yang, L. H. Zhang and H. J. Zhang, *J. Phys. Chem. C*, 2009, **113**, 16638.
31 L. Xu, C. L. Lu, Z. H. Zhang, X. Y. Yang and W. H. Hou, *Nanoscale*, 2010, **2**, 995.
32 Q. Kuang, Z. W. Lin, W. Lian, Z. Y. Jiang, Z. X. Xie, R. B. Huang and L. S. Zheng, *J. Solid State Chem.*, 2007, **180**, 1236.
33 C. X. Li and J. Lin, *J. Mater. Chem.*, 2010, **20**, 6831.
34 Z. J. Zhang, X. P. Xu, W. Y. Li, Y. M. Yao, Y. Zhang, Q. Shen and Y. J. Luo, *Inorg. Chem.*, 2009, **48**, 5715.
35 Z. L. Wang, J. H. Hao, H. L. W. Chan, G. L. Law, W. T. Wong, K. L. Wong, M. B. Murphy, T. Su, Z. H. Zhang and S. Q. Zeng, *Nanoscale*, 2011, 3, 2175.
36 L. Q. Liu and X. Y. Chen, *Nanotechnology*, 2007, 18.
37 X. Wang and Y. Li, *Angew. Chem. Int. Chem*., 2003, **42**, 3497.
38 J. Yang, C. Li, Z. Cheng, X. Zhang, Z. Quan, C. Zhang and J. Lin, *J. Phys. Chem. C*, 2007, **111**, 18148.
39 C. Louis, R. Bazzi, C. A. Marquette, J. L. Bridot, S. Roux, G. Ledoux, B. Mercier, L. Blum, P. Perriat and O. Tillement, *Chem. Mater*., 2005, **17**, 1673.
40 M. Nichkova, D. Dosev, S. J. Gee, B. D. Hammock and I. M. Kennedy, *Anal. Chem.*, 2005, **77**, 6864.
41 Y. H. Song, N. Guo and H. P. You, *Eur. J. Inorg. Chem.*, 2011, **14**, 2327.
42 G. Jia, H. P. You, K. Liu, Y. Zheng, N. Guo and H. Zhang, *Langmuir*, 2010, **26**, 5122.
43 G. Tian, Z. Gu, X. Liu, L. Zhou, W. Yin, L. Yan, S. Jin, W. Ren, G. Xing, S. Li and Y. Zhao, *J. Phys. Chem. C*, 2011, **115**, 23790.
44 P. Yang, S. Gai, Y. Liu, W. Wang, C. Li and J. Lin, *Inorg. Chem.*, 2011, **50**, 2182.
45 F. Q. Tang, L. L. Li and D. Chen, *Adv. Mater.*, 2012, 24, 1504.
46 Y. D. Xia and R. Mokaya, *Adv. Mater.*, 2004, **16**, 886.
47 T. Liu, Y. Wang, H. Qin, X. Bai, B. Dong, L. Sun and H. Song, *Mater. Res. Bull.*, 2011, **46**, 2296.
48 V. Bagalkot, L. Zhang, E. Levy-Nissenbaum, S. Jon, P. W. Kantoff, R. Langer and O. C. Farokhzad, *Nano Lett*., 2007, **7**, 3065.
49 S. Q. Liu, Y. W. Tong and Y. Y. Yang, *Biomaterials*, 2005, **26**, 5064.
50 Y. J. Gu and B. Yan, *Inorg. Chim. Acta*, 2013, **408**, 96.
51 S. Gai, P. Yang, D. Wang, C. Li, N. Niu, F. He and X. Li, *CrystEngComm*, 2011, **13**, 5480.
52 X. Kang, D. Yang, P. Ma, Y. Dai, M. Shang, D. Geng, Z. Cheng and J. Lin, *Langmuir*, 2013, **29**, 1286.
53 R. Lv, S. Gai, Y. Dai, N. Niu, F. He and P. Yang, *ACS Appl. Mat. Interfaces,* 2013, **5**, 10806.
54 H. Niu, Q. Min, Z. Tao, J. Song, C. Mao, S. Zhang and Q. Chen, *J. Alloys Compd*., 2011, **509**, 744.
55 J. L. Zhang, X. F. Yang, J. X. Fu, C. L. Liang, M. M. Wu, J. Wang, Q. Su, *Cryst. Growth Des*. 2013, **13**, 2292.
56 J. L. Zhuang, L. F. Liang, H. H. Y. Sung, X. F. Yang, M. M. Wu, I. D. Williams, S. H. Feng and Q. Su, *Inorg. Chem.*, 2007, **46**, 5404.
57 J. F. Wang, Y. M. Yao, Y. Zhang and Q. Shen, *Inorg. Chem.*, 2009, **48**, 744.
58 F. He, P. Yang, D. Wang, C. Li, N. Niu, S. Gai and M. Zhang, *Langmuir*, 2011, **27**, 5616.
59 Y. J. Cui, Y. F. Yue, G. D. Qian and B. L. Chen, *Chem. Rev*. , 2012, **112**, 1126.
60 S. V. Eliseeva and J. C. G. Bunzli, *Chem. Soc. Rev.*, 2010, **39**, 189.
61 G. S. Yi, H. C. Lu, S. Y. Zhao, G. Yue, W. J. Yang, D. P. Chen and L. H. Guo, *Nano Lett.*, 2004, **4**, 2191.
62 H. L. Sun, B. N. Guo, R. Cheng, F. H. Meng, H. Y. Liu and Z. Y. Zhong, *Biomaterials*, 2009, **30**, 6358.
63 R. Kumar, M. Nyk, T. Y. Ohulchanskyy, C. A. Flask and P. N. Prasad, *Adv. Funct. Mater*., 2009, **19**, 853.
64 Q. M. Wang and B. Yan, *J. Mater. Chem.*, 2004, **14**, 2450.
65 M. Yu, J. Lin and J. Fang, *Chem. Mater.*, 2005, **17**, 1783.
66 C. Wang, L. Cheng and Z. Liu, *Biomaterials*, 2011, **32**, 1110.
67 Y. S. Liu, D. T. Tu, H. M. Zhu and X. Y. Chen, *Chem. Soc. Rev*., 2013, **42**, 6924.
68 P. P. Yang, Z. W. Quan, Z. Y. Hou, C. X. Li, X. J. Kang, Z. Y. Cheng and J. Lin, *Biomaterials*, 2009, **30**, 4786.

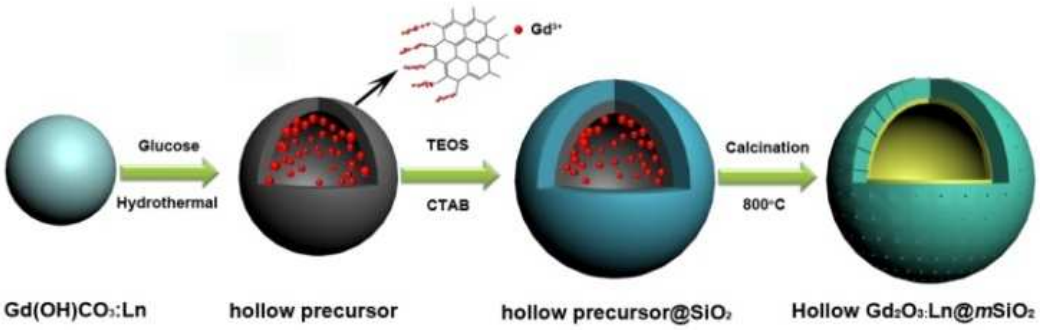

Core-shell structured Gd_2O_3:Ln@*m*SiO_2 hollow microspheres with interesting double-shell and mesoporous structure have been fabricated. The luminescent composite shows obvious drug storage and release properties.